Appl. Phys. A 60, 167–171 (1995)

Applied Physics A Materials Science & Processing

Aggregation of fractal and dendritic Ag clusters on a Pt(111) surface

H. Brune, H. Röder, C. Romainczyk, C. Boragno, K. Kern

Institut de Physique Expérimentale, EPF Lausanne, CH-1015 Lausanne, Switzerland
(Fax: +41-21/693-3604)

Received: 22 June 1994/Accepted: 13 September 1994

Abstract. We have used variable-temperature scanning tunneling microscopy to study the aggregation of two-dimensional Ag clusters on Pt(111). A transition from randomly ramified to dendritic fractal growth is observed in the diffusion-limited regime. Atomic-scale observations have identified the anisotropy of edge diffusion as microscopic origin of this crossover. Dependent on the deposition flux, this anisotropy is either amplified to the macroscopic-cluster shape and trigonal dendrites result, or it is degenerated and randomly ramified fractals occur. Our study elucidates the close relation between fractal and dendritic pattern formation in diffusion-limited aggregation on a two-dimensional lattice.

PACS: 68.70.+w; 61.43.Hv; 68.55.−a

The similarity of patterns formed in non-equilibrium growth processes in physics, chemistry and biology [1] is conspicuous and many attempts have been made to discover common mechanisms underlying their growth [2]. The central question in this context is what causes some patterns to be dendritic, as, e.g., snowflakes, while others grow fractal (randomly ramified), as, e.g., dielectric breakdown patterns [3]. In general, fractal growth is expected when randomness dominates, whereas dendritic growth is caused by the influence of anisotropy. In crystallographic growth, both, randomness (the random walk of atoms before they attach) and anisotropy (due to the lattice symmetry) are present. Accordingly, either random or ordered crystalline growth can be observed dependent on the exact growth conditions. In electrochemical deposition, e.g., a transition from fractal to dendritic growth is observed through variation of the growth speed [4, 5]. In analogy, here, we report a crossover from fractal to dendritic patterns for growth in two dimensions: the diffusion-limited aggregation of Ag atoms on a Pt(111) surface studied by means of variable-temperature STM (Scanning Tunneling Microscopy).

The direct experimental analogue to two-dimensional DLA (Diffusion-Limited Aggregation) simulations [6, 7] is vapour-phase epitaxy of metals on single-crystal metal surfaces at low temperatures: The film atoms, once adsorbed on the surface from the gas phase, diffuse in a random walk until they stick irreversibly to the perimeter of a growing aggregate. If perimeter diffusion is prohibited, the classical fractals result [8]. If a certain perimeter mobility is allowed and this mobility is anisotropic, however, deviations from this behaviour can occur, as will be demonstrated here. In our experiments, the parameters controlling growth are the temperature and flux of deposition, the first determines the perimeter mobility and the second the growth velocity.

The experiments were performed in ultrahigh vacuum with standard facilities for sample preparation and film evaporation. The Pt(111) crystal was cleaned by repeated cycles of Ar-ion bombardment (650 eV) at 830 K, annealing in oxygen atmosphere (880 K, 1×10^{-7} mbar) and subsequent flash to 1200 K. The Ag (purity 99.995%) aggregates were grown by vapour-phase epitaxy with an MBE-Knudsen cell at a background pressure better than 2×10^{-10} mbar. The STM images were recorded at isothermal conditions to Ag deposition because the cluster morphology is metastable.

The variable-temperature STM applied for this purpose is a home-built instrument which allows for measurements at temperatures ranging from 25 K to 800 K. It is based on the "Beetle"-type STM [9], where thermal drift is, to fist order, compensated by the fact that it stands on piezo legs which have equal thermal expansion rates as the single-tube scanner to which the tip is mounted. The sample is hat-shaped and it is clamped on its brim between a small copper disk and a molybdenum ring, which provides the ramps for the inertial approach [10]. For cooling, the Cu disk is connected to a liquid-He flux cryostat via a soft copper braid (diameter 4 mm, length 50 mm), which is untwisted into several single cords. Heating is done either by radiation or by electron bombardment from a filament located behind the sample. This small sample holder is rigidly mounted onto a big

cylindrical copper block which itself resides on viton spacers inside a steel tube [11]. The viton serves to damp external high-frequency vibrations. The mechanical vertical stability of the STM is 0.1 Å. No detectable change in stability is observed when the He flux is turned on, i.e., vibrations caused by the He flux at the cryostat are effectively decoupled from the sample by means of the soft Cu braid and the big Cu block where the sample is attached to.

The temperature desired is adjusted upon regulation of the filament current by a commercial PID controller. The temperature is measured by a thermocouple (NiCrNi, diameter 0.1 mm); its wires are spot-welded separately onto the brim of the crystal in order to ensure that the thermocouple "hot junction" is on the crystal [12]. The stability in temperature is 0.1 K, which is sufficient to reduce thermal drift in STM images below 5 nm/min. From nucleation studies at low temperatures [13] it is inferred that the absolute value measured for the temperature can be reproduced within 1 K between different experiments. In order to have quick access to different temperatures with the STM, i.e., to have small equilibration times of about 10 min, we took care to cool or heat only the sample (together with its small holder), i.e., for low temperatures the big Cu block as well as the STM basically stay at room temperature. For the Cu block this is achieved by the use of thin stainless-steel screws to mount the sample holder [12]. Figure 1 shows how the temperature of the STM's piezos changes with sample temperature. At low temperatures, where the radiative energy transfer is small, the piezo ceramics remain to a good approximation at room temperature (the thermal contact between piezos and the Mo ring via stainless-steel spheres is sufficiently bad). For sample temperatures above room temperature, radiative heating steadily increases the temperature of the piezo ceramics. In order to avoid their depolarization, we chose the upper limit for the sample temperature at 800 K where the piezos stay at 450 K.

For the STM images shown here ($-0.5\,\mathrm{V} \leq V_t \leq -1.5\,\mathrm{V}$, $1.0\,\mathrm{nA} \leq I_t \leq 3.0\,\mathrm{nA}$), the derivative $\partial z/\partial x$ of the lines of constant tunnel current has been recorded. They, therefore, represent the surface as it appears when illuminated from the left.

The two-dimensional Ag aggregates shown if Fig. 2 were grown at 110 K. The coverage of 0.12 monolayers

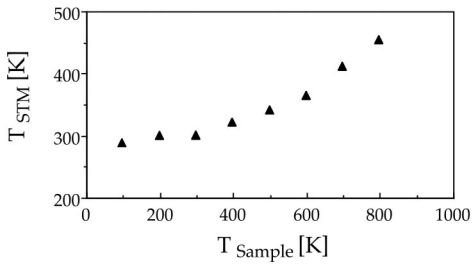

Fig. 1. Plot of the temperature measured at the piezo ceramics of the "Beetle"-type STM as a function of sample temperature. The temperatures are equilibrium values obtained after waiting for 1h

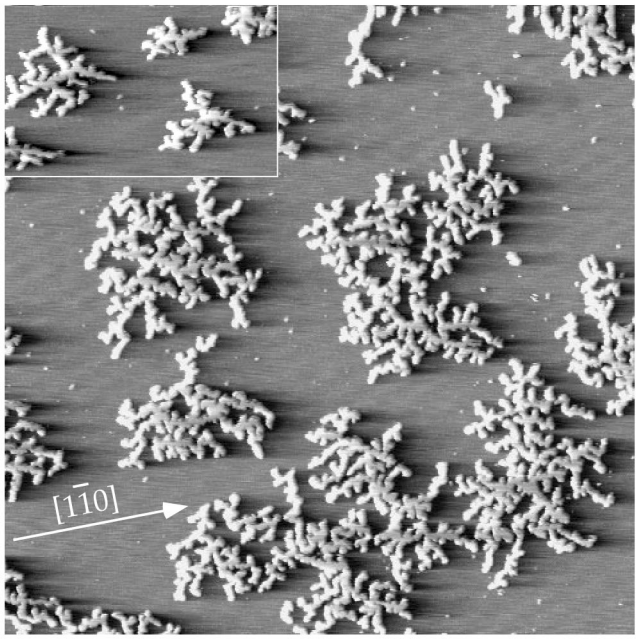

Fig. 2. STM image showing fractal (randomly ramified) Ag aggregates grown on Pt(111) at 110 K and a deposition flux of 1.6×10^{-5} ML/s (size: 1200 Å × 1200 Å, coverage: $\Theta = 0.12$ ML); inset: small dendritic islands obtained at 110 K and high flux (530 Å × 330 Å, $\Theta = 0.12$ ML, $R = 1.1 \times 10^{-3}$ ML/s)

(ML) was deposited at a very low Ag flux of 1.6×10^{-5} ML/s (1ML is defined as the density of the Pt(111) substrate of 1.50×10^{15} atoms/cm^2). Large clusters ($\approx$3000 Ag atoms) with an open ramified structure are formed under these conditions. The branches of the clusters frequently alter their direction of growth and thus show no long-range correlation with the trigonal substrate symmetry. The branches are of monoatomic height, their thickness is almost constant over the entire aggregate and much smaller than its radius of gyration. In fact, the arms are only 2 ± 1 atoms wide, as determined from the total arm length and the cluster size. (Branches are imaged 14 ± 1 Å wide in Fig. 2, which is consistent with their actual width if the finite curvature of the STM tip is taken into account.) The shape of the Ag aggregates grown at 110 K is very similar to that of fractal aggregates simulated with the classical DLA computer codes either performed off-lattice (no anisotropy) [7, 14] or on-lattice with noise dominating lattice anisotropy [6, 7]. Investigation of the fractal character of the Ag aggregates shown in Fig. 2 yields scaling over two orders of magnitude with a fractal dimension of $D = 1.76 \pm 0.07$ [15]. This experimental value is in good agreement with DLA simulations [6, 7].

A drastic change of the aggregate patterns is observed upon the use of a (by two orders of magnitude) increased flux. This is demonstrated in Fig. 3 showing Ag clusters (the biggest consists of $\approx$8000 atoms) grown at 130 K with the increased flux. A nice dendritic pattern is observed with the characteristic backbones, whose orientation is determined by the crystalline anisotropy of the substrate. In snow-flake terminology, this dendrite is of

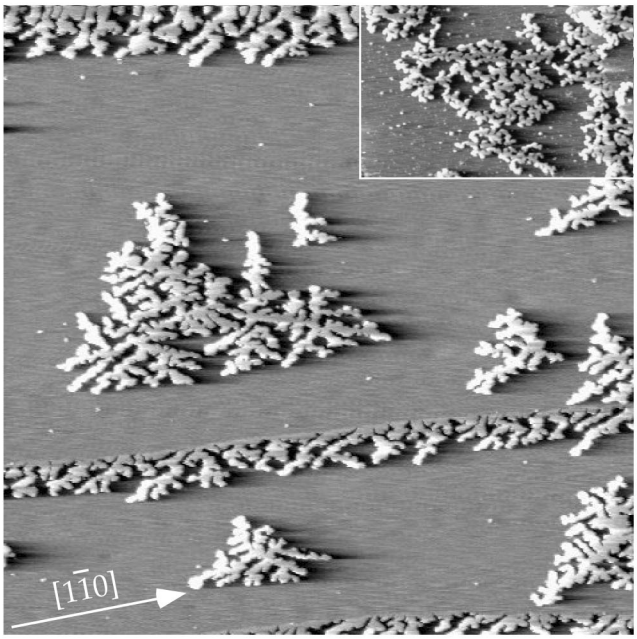

Fig. 3. STM image showing the dendritic shape of the Ag aggregates grown at 130 K with a flux of $R = 1.1 \times 10^{-3}$ ML/s (1200 Å × 1200 Å, $\Theta = 0.12$ ML); inset: transition from dendritic to fractal growth at 130 K upon lowering the deposition flux by two orders of magnitude (830 Å × 520 Å, $\Theta = 0.12$ ML, $R = 1.6 \times 10^{-5}$ ML/s)

the *P2a* type (plane *P*, with irregular number of branches 2, three branched *a*) [16]. The three axes of preferred growth of the dendrite are oriented along the crystallographic $\langle 11\bar{2} \rangle$-directions of the substrate. While the qualitative growth form has changed dramatically, the fractal dimension is nearly unaffected. We find $D = 1.77 \pm 0.05$ for the biggest cluster in Fig. 3, which agrees with that of the randomly ramified aggregates of Fig. 2. This is expected from DLA for the relatively small cluster sizes under consideration here [17].

It is important to notice that the slight increase in temperature to 130 K chosen for Fig. 3 (in order to obtain clusters with comparable size to those in Fig. 2) has no influence on the cluster shape. The inset in Fig. 3 shows that also at 130 K randomly ramified patterns with no preferred-orientation result through the application of the low flux. On the other hand, dendrites also grow at 110 K upon deposition with the high flux used in Fig. 3 (see inset in Fig. 2). Therefore, the parameter that drives the crossover from ramified to dendritic patterns is the deposition flux, i.e., the growth speed of the aggregate.

These observations are in full agreement with earlier work. Increasing the growth speed (Zn^{2+} concentration and voltage) in electrochemical deposition resulted in a transition from fractal to dendritic patterns [4, 5]. In the propagation of a low viscous medium into a high viscous one in a Hele-Shaw cell [18] from certain propagation speeds on, viscous fingering occurs (Saffman-Taylor instability [19]). The dynamics is dominated by tip bifurcations which lead to randomly branched structures. When anisotropy is introduced into these systems, either by scratching a lattice into one of the glass plates of the Hele-Shaw cell [20, 21], or by use of a liquid crystal as high viscous medium [22], a transition from randomly ramified to dendritic patterns is found. This transition takes place upon increase of the expansion rate, which, again is in accordance with the results presented above. The hydrodynamic experiments, however, nicely demonstrate that anisotropy is a necessary condition for dendritic growth, a result which has also been found in statistical-mechanics simulations of these experiments [23, 24]. Similarly, in DLA work, this transition from fractal to dendritic patterns is obtained when anisotropy dominates noise [3, 14, 25, 26]. The microscopic mechanism that establishes anisotropy only at increased growth rates to the macroscopic pattern shape, however, can be analyzed for the present system.

From comparison with DLA work, it is found that the anisotropy that characterizes the Ag dendrites consists in growth preferentially taking place in only three of the six $\langle 11\bar{2} \rangle$-directions of the substrate [17]. The nature of this anisotropy for growth of Ag on Pt(111) is linked to the trigonal symmetry of this surface. A densely packed cluster on an fcc-(111) surface is bound by two types of edges with atomically different structure (*A* and *B* edges).

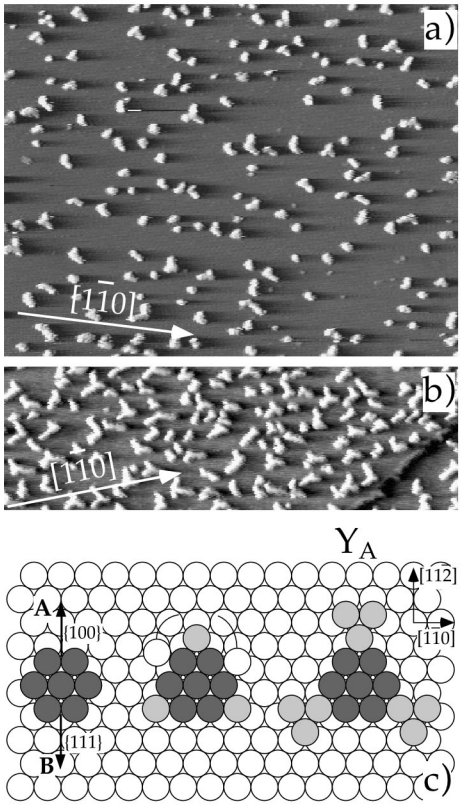

Fig. 4a–c. STM images of small Ag_n clusters grown on Pt(111) at 80 K with the average cluster size being $n = 13$ in (**a**) and $n = 21$ atoms in (**b**), respectively; (**a**): 600 Å × 470 Å, $\Theta = 0.037$ ML, $R = 3.7 \times 10^{-4}$ ML/s, (**b**): 600 Å × 190 Å, $\Theta = 0.12$ ML, $R = 3.6 \times 10^{-3}$ ML/s); (**c**) schematic model showing the growth of a heptamer to a Y_A

A edges are {100} facets, whereas B edges are {111} facets (see the heptamer on the left-hand side in Fig. 4c). This microscopic difference is partly reflected in a different activation barrier for perimeter diffusion. In order to identify which of the close-packed Ag-edge orientations is of A- and which one of B-type, it is important to notice that Ag resides up to one monolayer on fcc sites on the Pt(111) surface. This site can be deduced from the perfect, i.e., dislocation-free attachment of Ag islands to the neighbouring Pt layer at ascending steps: STM images would reveal an undulation if there was a stacking fault [27]. However, the fact that the Ag islands are imaged as a perfectly flat layer where they are connected to Pt steps (see, e.g., Ag at the step in Fig. 3) demonstrates the absence of a stacking fault and thus the fcc-adsorption site for Ag. In accordance, for a comparable system, i.e., Ag/Pd(111) [lattice mismatch 5.1% versus 4.5% for Ag/Pt(111)], the fcc site has also been found for the first monolayer [28]. For Ag/Pt(111), growth experiments analogous to those by Michely et al. [29] show that diffusion along B steps is faster than along A steps at $T < 200$ K and, thus, the former has a lower activation barrier. Interestingly, this is inverse to what is known for homoepitaxial systems [30]. This difference might be due to strain, which preferentially is relieved at steps where the atoms have lower coordination. This might shift their position apart from the ideal hollow site and/or modify the electronic structure at the step, which both is expected to have consequennces on the migration of a Ag atom along a step.

The difference in migration along the two types of steps is a kinetic effect and, thus, especially pronounced at low temperature. Figures 4a and b show the initial branching of the cluster seed at 80 K. The smaller islands are imaged almost spherical in Fig. 4a. From their shape and the island-size distribution, it can be concluded that those small islands are heptamers, they constitute the seed particle. The biggest islands are forming Ys with arms 120° apart. Y-branching of the heptamer is possible in two ways: by adding Ag adatoms to its A steps or to its B steps (labelled Y_A and Y_B, respectively, the Y_A-type is shown in Fig. 4c). The two types of Y s differ by a rotation of 60°. In the experiment, we exclusively observe the Y_A cluster. Therefore, growth occurs predominantly in the three directions perpendicular to A steps with the result that only one orientation of the Ys occurs. The brances of the Ys are exactly in the preferred growth directions found for the bigger dendrite at 130 K.

This anisotropy in growth is even better seen for somewhat bigger clusters, as shown in Fig. 4b (notice the different orientation of the crystallographic $[1\bar{1}0]$-direction compared to Fig. 4a). Because Ag atoms arrive at random at each edge orientation, the fact that we find only the Y_A-type must invoke perimeter diffusion along B steps, whereas diffusion along A steps is frozen in.

There is, however, a second necessary condition for the observed growth of Y_As that applies after the addition of the first three atoms to the heptamer (which is most plausibly done at A steps): The Ag_{10} aggregate is then exclusively bound by B steps. In order to grow a stable expansion in A-direction, as observed, two diffusing perimeter atoms have to meet each other at the aggregate's corners (see Fig. 4c). Such an event, however, is the more probable the more diffusing atoms similarly in the sence: at the same time are present at the island perimeter. Their quantity is directly related to the flux. The number of atoms arriving per second at the island perimeter can be estimated as follows. Every island has an "active" area related to it, i.e., all atoms arriving onto this area, will, on the average, perform their random walk towards the island. At saturation of the island density (which is the case for the coverages shown here), this area is given by 1/ island density. The flux onto it in atoms per second is the deposition flux times this area. At the high flux used in Fig. 3, there are on the average 100 atoms arriving per second at the aggregate's perimeter, whereas there is only one per second at the low flux in Fig. 2. In addition, the mean free path of a diffusing perimeter atom increases only with square root of the diffusion time (one dimensional random walk). Therefore, the probability for two atoms to meet at a corner is more probable at increased flux, and, due to faster migration along B steps, also much more probable at those corners that point in A-direction. Thus, dendrites with trigonal growth perpen dicular to A steps are formed for high flux. At low flux, on the other hand, interaction of two diffusing particles at the island corner is less probable and predominantly single non-interacting mobile atoms are present at the step. Therefore, anisotropy looses more of its importance in favour of noise and the aggregate grows randomly.

A mechanism equally possible for the transition to random growth at low flux is that cluster aggregation could take place under these conditions. The mobility of Ag dimers on Pt(111) is indeed expected to be in the range where they could contribute to the aggregation process. An estimation based on the data for Ir clusters on Ir(111) [30], and on the diffusion barrier for Ag atoms on Pt(111) [13], yields jump frequencies for Ag dimers of $7\ s^{-1}$ and $400\ s^{-1}$ at 110 K and 130 K, respectively. It is expected that the contribution of dimers to the aggregation process is increased as the growth speed is lowered. It is evident that the perimeter mobility of a dimer is substantially decreased with respect to that of an atom. Therefore, if dimer aggregation would be dominant at the low flux, this would freeze-in perimeter mobility and thus lead to DLA clusters. At the high growth rate, on the other hand, predominantly monomers attach to the growing aggregate. They obey the above-described anisotropic perimeter diffusion which leads to dendrites. Whether dimer aggregation occurs at the low growth rates or the interaction of mobile atoms at the perimeter becomes less probable, leading to a degeneracy of diffusion anisotropy, has to be further explored.

In summary, we have demonstrated a transition from fractal to dendritic growth in surface aggregation driven by the growth rate. The mechanism responsible for dendritic growth at high flux has been identified as the anisotropy in edge diffusion for attaching Ag atoms.

Acknowledgement. This research is supported by the Schweizerische Nationalfond.

References

1. E. Ben-Jacob, O. Schochet, A. Tenebaum, I. Cohen, A. Czirok, T. Vicsek: Nature **368**, 46 (1994)
2. H. Takayasu: *Fractals in the Physical Sciences* (Manchester Univ. Press, Manchester 1990)
3. T. Vicsek: *Fractal Growth Phenomena* (World Scientific, Signapore 1989)
4. Y. Sawada, A. Dougherty, J.P. Gollub: Phys. Rev. Lett. **56**, 1260 (1986)
5. D. Grier, E. Ben-Jacob, R. Clarke, L.M. Sander: Phys. Rev. Lett. **56**, 1264 (1986)
6. T.A. Witten, L.M. Sander: Phys. Rev. Lett. **47**, 1400 (1981)
7. P. Meakin: Phys. Rev. A **27**, 1495 (1983)
8. R.Q. Hwang, J. Schröder, C. Günther, R.J. Behm: Phys. Rev. Lett. **67**, 3279 (1991)
9. K. Besocke: Surf. Sci. **181**, 145 (1987)
10. J. Frohn, J.F. Wolf, K. Besocke, M. Teske: Rev. Sci. Instrum. **60**, 1200 (1989)
11. T. Michely, G. Comsa: Surf. Sci. **256**, 217 (1991)
12. R. David, K. Kern, P. Zeppenfeld, G. Comsa: Rev. Sci. Instrum. **57**, 2771 (1986)
13. H. Brune, H. Roeder, C. Boragno, K. Kern: Phys. Rev. Lett. **73**, 1955 (1994)
14. J.P. Eckmann, P. Meakin, I. Procaccia, R. Zeitak: Phys. Rev. Lett. **65**, 52 (1990)
15. H. Brune, C. Romainczyk, H. Röder, K. Kern: Nature **369**, 469 (1994)
16. U. Nakaya: Snow Crystals (Harvard Univ. Press, Cambridge 1954)
17. P. Meakin: Phys. Rev. A **33**, 3371 (1986)
18. H.S.S. Hele-Shaw: Nature **58**, 34 (1898)
19. P.G. Saffman, G.J. Taylor: Proc. R. Soc. London, Ser. A **245**, 312 (1958)
20. E. Ben-Jacob, R. Godbey, N.D. Goldenfeld, J. Koplik, H. Levine, T. Mueller, L.M. Sander: Phys. Rev. Lett. **55**, 1315 (1985)
21. V. Horváth, T. Vicsek, J. Kertész: Phys. Rev. A **35**, 2353 (1987)
22. A. Buka, J. Kertész, T. Vicsek: Nature **323**, 424 (1986)
23. J. Nittmann, H.E. Stanley: Nature **321**, 663 (1986)
24. J. Nittmann, H.E. Stanley: J. Phys. A **20**, L1185 (1987)
25. P. Meakin: Phys. Rev. A **36**, 332 (1987)
26. J.P. Eckmann, P. Meakin, I. Procaccia, R. Zeitak: Phys. Rev. A **39**, 3185 (1989)
27. H. Brune, H. Röder, C. Boragno, K. Kern: Phys. Rev. B **49**, 2997 (1994)
28. B. Eisenhut, J. Stober, G. Rangelov, Th. Fauster: Phys. Rev. B **47**, 12980 (1993)
29. T. Michely, M. Hohage, M. Bott, G. Comsa: Phys. Rev. Lett. **70**, 3943 (1993)
30. G. Ehrlich: Surf. Sci. **246**, 1 (1991)